

The Effect of Acetic Acid on the Localized Corrosion of 3Cr Steel in the CO₂-saturated Oilfield Formation Water

Kexi Liao¹, Jihui Leng¹, Qiang Huang², Lihui Yang², Feilong Zhou^{1,*}, Shuai Zhao¹, Xin Liu¹

¹ Petroleum Engineering School, Southwest Petroleum University, Chengdu 610500, China;

² Xinjiang Petroleum Engineering Co. LTD, Karamay 834000, China;

*E-mail: 1966258106@qq.com

Received: 7 April 2020 / Accepted: 26 May 2020 / Published: 10 August 2020

The effect of acetic acid on the localized corrosion of 3Cr steel in the CO₂-saturated oilfield formation water was investigated using weight loss tests, surface characterization, and electrochemical measurements. Weight loss tests revealed that acetic acid and increased concentration can dramatically accelerate the general rate of 3Cr steel when the general corrosion rate increased from 0.2841 to 1.2236 mm/y in tandem with an increase in the acetic acid concentration from 0 to 5,000 ppm. Surface characterization measurements were performed by scanning electron microscopy, energy-dispersive X-ray spectroscopy, X-ray powder diffraction, and three-dimensional profilometry. The results revealed that FeCO₃ and Cr compounds dominated the corrosion scales and that the corrosion scales gradually became looser and shed off with increased acetic acid concentration. The localized corrosion rate increased from 0.2663 to 4.2416 mm/y in tandem with an increase in acetic acid concentration from 0 to 5,000 ppm. The electrochemical measurements showed that the reduced reaction of undissociated acetic acid in the solution participated in the cathodic reaction process. Moreover, acetic acid was shown to affect the adsorption process of the corrosion product scales, with the entire corrosion reaction drastically accelerating. In this paper, the localized corrosion mechanism of 3Cr steel in the CO₂-saturated oilfield formation water is discussed. Acetic acid significantly contributes to the generation of localized corrosion. Moreover, the combined effect of Cl⁻ stimulates the formation and development of localized corrosion on 3Cr steel's surface.

Keywords: acetic acid, CO₂-saturated oilfield formation water, 3Cr steel, localized corrosion, localized corrosion depth.

1. INTRODUCTION

In the oil and gas industry, carbon steels are commonly used in pipeline materials owing to their low cost [1]. However, carbon steels often suffer from localized corrosion in a CO₂ environment, especially when containing organic acids [2]. This would accelerate the failure of the pipeline. However,

3Cr steel has received a great deal of attention because it not only improves the CO₂ corrosion resistance by 3–10 times but also maintains the cost within 1.5 times compared with conventional carbon steels of the same grade [3,4,5]. Many previous studies have attributed the higher corrosion resistance of 3Cr steel vis-à-vis CO₂ corrosion to Cr enrichment in corrosion scales, which results in denser corrosion scales and lower susceptibility to localized corrosion [6,7,8].

The CO₂ corrosion rules, mechanism, and prediction model have been extensively investigated in the past decades [9,10,11,12]. Various organic acids, such as formic acid, acetic acid, and propionic acid, can be observed in CO₂-saturated oilfield formation water. Acetic acid is the most abundant acid and accounts for 50%–90% of organic acids [13]. However, acetic acid can considerably accelerate the corrosiveness of the solution and make the corrosion process more complicated.

To date, some research has been conducted on the effect of acetic acid on the corrosion of carbon steel in a CO₂ solution; however, the mechanism of its corrosion reaction remains controversial. Crolet [14] argued that the presence of acetic acid in a solution inhibits the corrosion process of steel due to its effect on anodic dissolution reaction. Zhang [15] pointed out that acetic acid in formation water expedites the cathodic reaction due to a direct reduction in undissociated acetic acid. Zhu [11] demonstrated that the addition of acetic acid can stimulate the cathodic reactions of N80 steel but inhibit the anodic reactions in CO₂-saturated oilfield formation water.

Other studies have shown that acetic acid can trigger a localized corrosion attack. However, there is limited consensus on its corrosion mechanism, and the corrosion law has not to date been studied quantitatively. Nafday and Nešić [16] pointed out that acetic acid can barely protect the FeCO₃ corrosion scale and cause localized corrosion. Okafor and Nešić [17] stated that acetic acid causes localized corrosion on the destructiveness of the FeCO₃ corrosion scale. Moreover, limited quantitative research on localized corrosion under the influence of acetic acid concentration has been reported, the study of which deserves more attention.

The CO₂-saturated oilfield formation water of an oilfield contains acetic acid, NaCl, NaHCO₃, CaCl₂, MgCl₂·6H₂O, and Na₂SO₄. The composition of CO₂-saturated oilfield formation water indicates its great possibility of causing corrosion on the steel pipe surface, and different concentrations of acetic acid have different impact sizes on the localized corrosion of pipelines. Therefore, research on the corrosion of metal materials in the CO₂-saturated oilfield formation water containing acetic acid is essential for the safe operation of pipelines.

In this work, the corrosion behaviors of 3Cr steel in the CO₂-saturated oilfield formation water with different acetic acid concentrations were investigated, employing weight loss tests, electrochemical measurements, surface characterization techniques, and three-dimensional (3D) profilometry. This article aimed to (1) reveal the corrosion behaviors of 3Cr steel in the presence or absence of acetic acid, (2) research the uniform corrosion behaviors of 3Cr steel with different acetic acid concentrations, and (3) study the effect of acetic acid concentration on localized corrosion of 3Cr steel and discuss the localized corrosion mechanism model.

2. EXPERIMENTAL

2.1 Materials and solution

A 3Cr steel pipeline with a composition (mass fraction) of 0.07% C, 0.20% Si, 0.53% Mn, 0.010% P, 0.005% S, 3.01% Cr, 0.20% Mo, 0.04% Nb, and Fe balance was used in the experiment. The specimens were cut into $10 \times 10 \times 3$ mm for the electrochemical tests. The unexposed areas and edges were coated with epoxy resin, leaving an exposed working area of 1 cm^2 . The specimens for the immersion tests were cut into $50 \times 10 \times 3$ mm. The composition of the test solution after the formation water in the oilfield is presented in Table 1. All specimens were sequentially ground with silicon carbide paper (from 240 to 1000 grit) and rinsed with deionized water and mineral ether. Then, the specimens were placed in a desiccator for around 24 h to remove the water.

Table 1. Chemical composition of the oilfield's formation water

Composition	NaCl	NaHCO ₃	CaCl ₂	MgCl ₂ ·6H ₂ O	Na ₂ SO ₄
Content (mg/L)	7704.7	2608.6	346.5	294.4	198.8

2.2 Electrochemical measurements

Electrochemical measurements were performed in a typical three-electrode cell through the EG&G potentiostat/galvanostat system (CS350). The working electrode was a 3Cr steel specimen. The reference and counter electrodes were a saturated calomel electrode (SCE) and a graphite rod, respectively. Electrochemical impedance spectroscopy (EIS) was measured at a frequency range of 100 to 10 MHz with an applied AC signal of 5 mV, whereas the 3Cr steel had an open circuit potential. Potentiodynamic polarization curves were measured, with a potential scan rate of 1 mV/s.

ZSimpWin and Cview were used to fit the EIS results and analyze the polarization curves. The details of the electrochemical measurements are as follows: five acetic acid concentrations of 0; 1,000; 2,000; 3,000; and 5,000 ppm. Before the tests, the solution was deoxygenated by purging CO₂ for 4 h. CO₂ purging continued throughout the test to minimize the possibility of air ingress [18]. The test temperature was 50°C.

2.3 Weight loss tests

Weight loss tests were conducted using an autoclave (5L) at 50°C and atmospheric pressure. In the simulating oilfield formation water, the acetic acid concentrations were 0; 1,000; 2,000; 3,000; and 5,000 ppm. Five parallel specimens were used in each group of experiments. Three were used for weight loss testing, one for X-ray diffraction (XRD) product analysis and the localized corrosion depth test, and one for surface morphology observation and the elemental composition test.

Before the experiment, the three specimens for weight loss tests were taken out from the desiccator and weighed using a balance with a precision of 0.1 mg. The simulating oilfield formation water (3L) was poured into the autoclave, and the solution was deoxygenated by purging CO₂ for 4 h. Subsequently, the specimens were hung on the holder and immersed in the solution. CO₂ purging continued throughout the test, and the test lasted 120 h.

Afterward, all the corroded specimens remained for the next corrosion rate tests and product characterization. The three specimens were descaled in a descaling liquid composed of hexamethylenetetramine (3.5 g), hydrochloric acid (500 mL), and deionized water (500 mL). as per ISO 8407: 2009 [19]. Then, the three specimens were rinsed, dried, and weighed again. The general corrosion rate was calculated using Eq. (1) [12]:

$$v = \frac{87600(m_1 - m_2)}{\rho S t} \quad (1)$$

where ρ is the density of 3Cr steel, g/cm³; S is the surface area of a specimen, cm²; t represents the test time, h; m_1 and m_2 represent the mass losses, g; 87,600 is the unit conversion constant; and v is the corrosion rate, mm/y.

2.4 Microstructure observation

The morphologies and elemental compositions of the 3Cr surface were characterized by scanning electron microscopy and energy-dispersive X-ray spectroscopy (EDS) (ZEISS EV0 MA15). The corrosion scale compositions were identified using XRD, with a Cu-K α X-ray source (X'Pert Pro). The corrosion product on the surface of the specimen was cleaned using the descaling liquid, and the surface of the steel substrate was tested using 3D profilometry (Bruker ContourGT). Based on the results of 3D profilometry, the localized corrosion rate (RL) and the pitting ratio (PR) were calculated using Eqs. (2) and (3) [20], respectively:

$$R_L = \frac{0.365h}{t} \quad (2)$$

where R_L denotes the localized corrosion rate, mm/y; t represents the test time, d; and h represents the maximum localized corrosion depth.

$$PR = \frac{P}{d} \quad (3)$$

where PR denotes the pitting ratio; p is the maximum localized corrosion depth, mm; d is the average corrosion depth, mm; and d is based on the results of the weight loss tests. The closer the PR is to 1, the closer the corrosion pattern is to uniform corrosion.

3. RESULTS

3.1 Weight loss tests

Figure 1 presents the general corrosion rate of 3Cr steel at 50°C in the simulating CO₂-saturated oilfield formation water with different acetic acid concentrations. The general corrosion rate of 3Cr steel is 0.2841 mm/y without acetic acid. As the concentration of acetic acid increased from 0 to 5,000 ppm, the

general corrosion rate increased from 0.2841 to 1.2236 mm/y. These trends are similar to the findings of Jia [21] who discovered that as the acetic acid concentration increases, the corrosion rate sharply increases, suggesting that acetic acid accelerates the process of CO₂ corrosion.

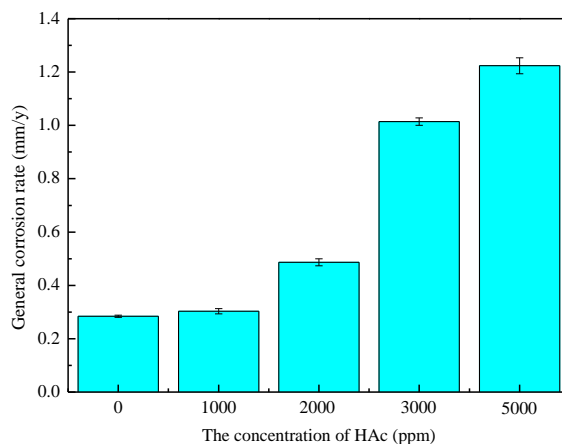


Figure 1. Corrosion rate of 3Cr steel at 50°C in the simulating CO₂-saturated oilfield formation water with different acetic acid concentrations

3.2 Microscopic morphologies and composition of surface scales

Figure 2 presents the microscopic morphologies and the composition of surface scales of 3Cr steel at 50°C in the simulating CO₂-saturated oilfield formation water with different acetic acid concentrations. At 0 ppm acetic acid concentration, the corrosion scales covering the surface of the 3Cr steel specimen were dense and invariably close. This finding is in agreement with that of Guo [6] who found that cracks caused by the dehydration effect of corrosion scales were scattered across the surface of the 3Cr steel [22]. At 1,000 ppm, the corrosion scale surface gradually became loose and porous and lost its protective properties. At 2,000 ppm, cracks appeared on the corrosion scale surfaces. At 3,000 ppm, the corrosion scales gradually shed off. As the acetic acid concentration increased to 5,000 ppm, serious delamination phenomena began to occur on the surfaces of the corrosion scales, indicating that the higher the acetic acid concentration, the more severe the corrosion. Figure 2(f) shows that the elements contained in the corrosion scales at different acetic acid concentrations are the same C, O, Fe, Cr element, indicating the similarity of the composition of the corrosion scales in different acetic acid concentrations.

Table 2 presents the specific element amount of corrosion scales of the 3Cr steel surface at 50°C in the simulating CO₂-saturated oilfield formation water with different acetic acid concentrations. According to the results of the EDS analysis, Fe amounts increased slightly, whereas C amounts remained roughly constant; moreover, both O and Cr amounts increased first before decreasing again. The proportion of Cr element was higher than 3%, suggesting that the corrosion scale composition may contain Cr oxides. Points E and F in Fig. 2(e) at 5,000 ppm acetic acid concentration are worth noting. Cr amounts were 9.01% and 20.82%. Moreover, serious uneven distributions of Cr elements occurred, affecting the occurrence of localized corrosion on the steel.

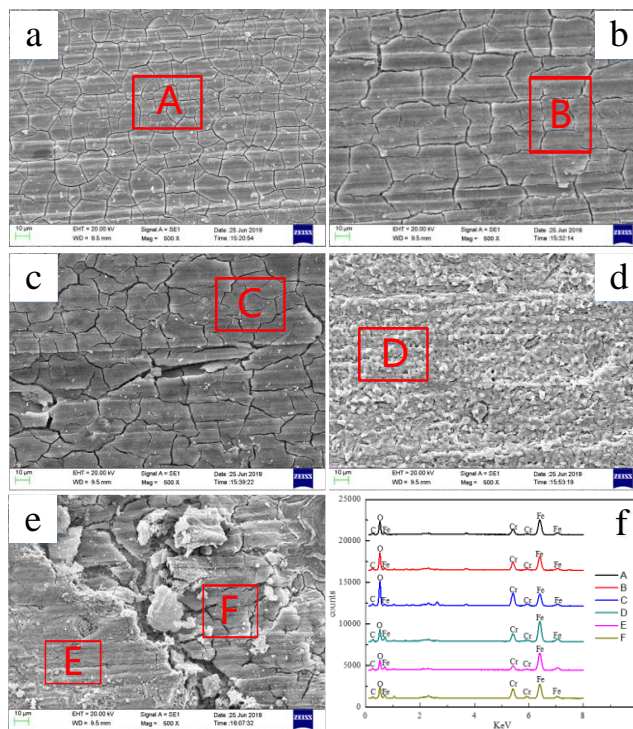


Figure 2. Microscopic morphologies and element composition of surface scales of 3Cr steel at 50°C in the simulating CO₂-saturated oilfield formation water with different acetic acid concentrations: (a) 0 ppm; (b) 1,000 ppm; (c) 2,000 ppm; (d) 3,000 ppm; (e) 5,000 ppm; (f) composition of surface scales

Table 2. Element amounts of corrosion scales in different solutions of acetic acid concentrations (wt%)

Acetic acid concentration (ppm)	Test position	Fe	C	O	Cr
0	A	45.01	11.17	30.35	11.53
1000	B	41.08	11.07	32.22	15.63
2000	C	30.43	11.03	36.12	22.43
3000	D	54.18	11.92	20.46	13.44
5000	E	57.86	12.41	20.72	9.01
5000	F	45.67	11.00	22.51	20.82

To further characterize the material composition of the corrosion scales with and without acetic acid, the corrosion scales of 0 and 3,000 ppm acetic acid concentration were selected for the XRD pattern analysis. Figure 3 presents the XRD patterns of the corrosion scales of the 3Cr steel substrate at 50°C in the simulating CO₂-saturated oilfield formation water with 0 and 3,000 ppm acetic acid concentration. The main peaks are iron peak and iron carbonate peak. Arguably, iron carbonate is the dominant component of the corrosion scale. This result is similar to those of Nazari [18]. Meanwhile, the result indicates that acetic acid concentration barely has any effect on the phase analysis of the corrosion scales.

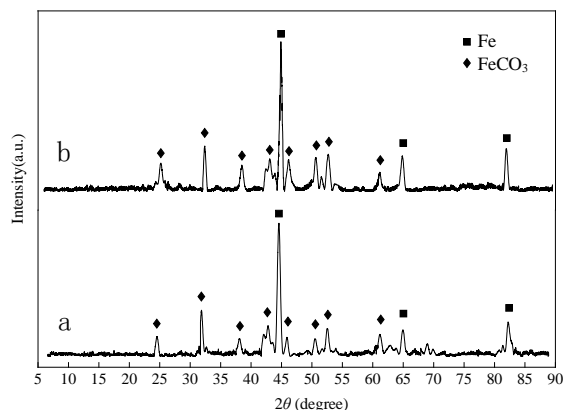
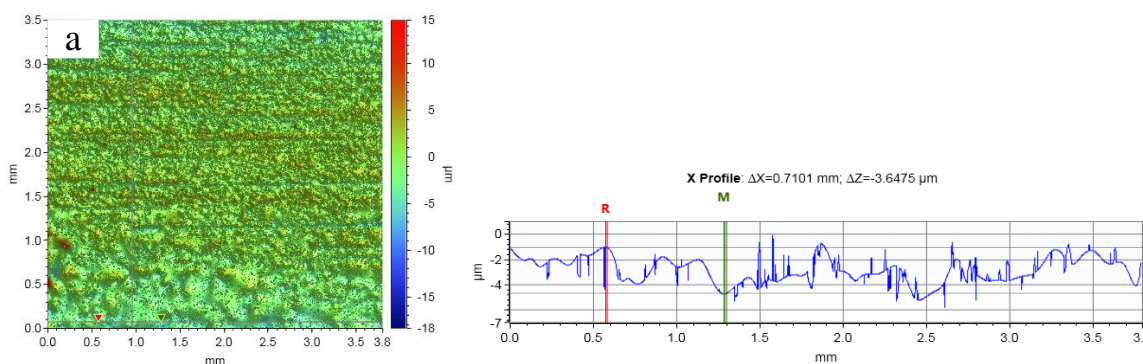


Figure 3. XRD patterns of the 3Cr steel substrate at 50°C in the simulating CO₂-saturated oilfield formation water with different acetic acid concentrations: (a) 0 ppm; (b) 3,000 ppm

3.3 Depth of localized corrosion defects

Figure 4 presents the 3D profilometry image of the 3Cr steel substrate at 50°C in the simulating CO₂-saturated oilfield formation water with different acetic acid concentrations. In the saturated carbon dioxide solution without acetic acid, the corrosion depth of the steel substrate surface was almost uniform, and the depth was shallow, maintaining minimal change. Moreover, the depth of corrosion ΔZ reached 3.6475 μM , indicating a form of uniform corrosion. The addition of acetic acid contributed to the unevenness of the small pits on the steel surface, and the number and area of the pits increased sharply in tandem with an increase in the acetic acid concentration. When the acetic acid concentration reached 3,000 ppm, small pits gradually developed a large pit, and the depth deepened, reaching 31.5783 μM . Severe uneven distribution of corrosion pits appeared at 5,000 ppm, and the depth of localized corrosion defects increased to 58.1044 μM .



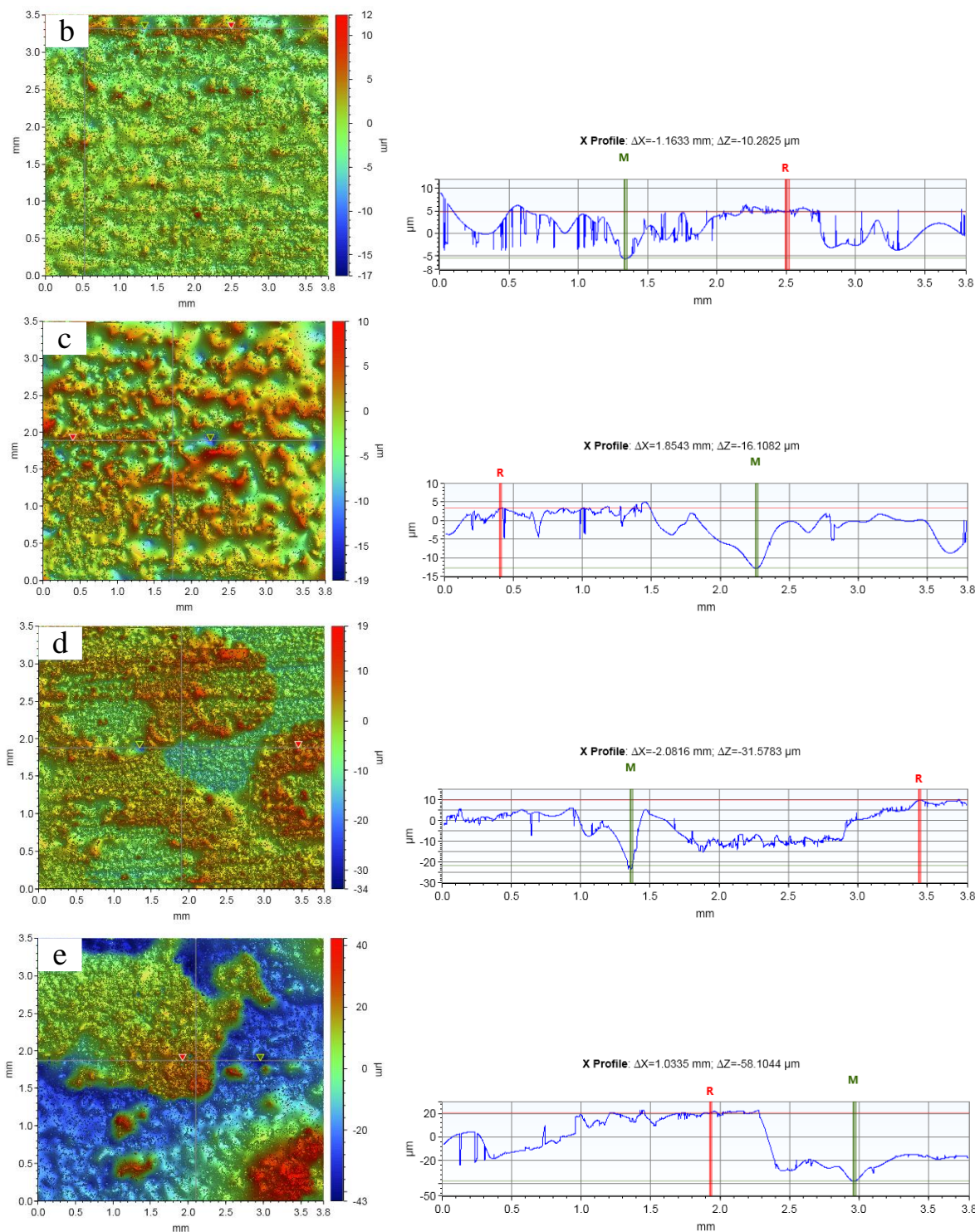


Figure 4. Specimen profilometry images of the 3Cr steel substrate at 50°C in the simulating CO₂-saturated oilfield formation water with different acetic acid concentrations: (a) 0 ppm; (b) 1,000 ppm; (c) 2,000 ppm; (d) 3,000 ppm; (e) 5,000 ppm

To further describe the change in the localized corrosion defects of the 3Cr steel substrate at 50°C in the simulating CO₂-saturated oilfield formation water with different acetic acid concentrations, Fig. 5 and Fig. 6 present the localized corrosion rates and the PR calculated using Eqs. (2) and (3), respectively.

According to Fig. 5, the localized corrosion rate increased in tandem with an increase in acetic acid concentration. Moreover, the localized corrosion rate rose dramatically compared with the general

corrosion rate. As the acetic acid concentration increased from 0 to 5,000 ppm, the localized corrosion rate increased from 0.2663 to 4.2416 mm/y. The results of this work confirm the effect of acetic acid concentration on the severity of the 3Cr steel localized corrosion from a quantitative perspective.

Figure 6 presents the PR of the 3Cr steel substrate at 50°C in the simulating CO₂-saturated oilfield formation water with different acetic acid concentrations. At 0 ppm acetic acid, the PR value was close to 1, indicating the closeness of the corrosion pattern to uniform corrosion, which is similar to the results of microscopic morphologies and 3D profilometry images. When acetic acid was added to the solution, the PR value reached 2 and deviated far from 1, even exceeding 3 at 5,000 ppm. The acetic acid concentration can be inferred to affect the corrosion process, with the high acetic acid concentration easily leading to localized corrosion.

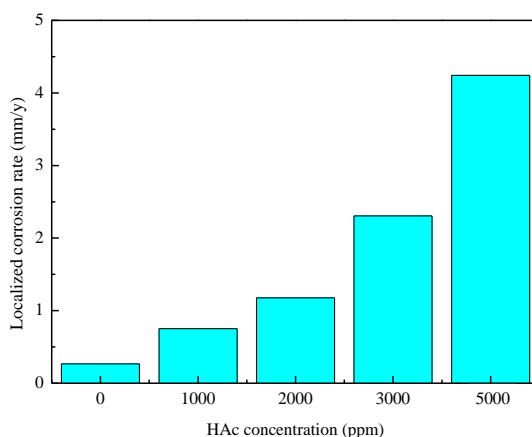


Figure 5. Localized corrosion rate of the 3Cr steel substrate at 50°C in the simulating CO₂-saturated oilfield formation water with different acetic acid concentrations

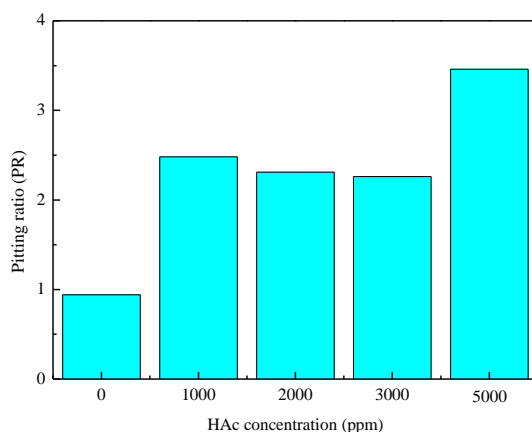


Figure 6. PR of the 3Cr steel substrate at 50°C in the simulating CO₂-saturated oilfield formation water with different acetic acid concentrations

3.4 Electrochemical measurements

Figure 7 presents the polarization curves of 3Cr steel at 50°C in the CO₂-saturated oilfield formation water with different acetic acid concentrations. The cathodic current density of the specimen

without acetic acid is lower than that with acetic acid. The addition of acetic acid moved the corrosion potential toward the positive direction, and the cathodic current density increased. This trend became more pronounced as the acetic acid concentration increased. However, the change in the anodic reaction was not obvious all the time, indicating that the addition of acetic acid stimulated the corrosion reaction, especially the cathodic reaction. These findings are similar to those of Nazari [23], who reported that the addition of acetic acid considerably shifts the corrosion potential in the cathodic current density, with minimal effect on the anodic side; moreover, the predominant cathodic reaction tends to reduce HAc. Table 3 presents the changes in electrochemical parameters with different acetic acid concentrations, such as corrosion potential (E_i), anodic Tafel slopes (b_a), cathodic Tafel slopes (b_c), and corrosion current density (i_{corr}). Table 3 shows that the corrosion current density increased in tandem with an increase in the acetic acid concentration, which is consistent with the weight loss results. Moreover, the cathode Tafel slope (b_c) is greater than the anode Tafel slope (b_a), and the corrosion reaction process is controlled by the cathode.

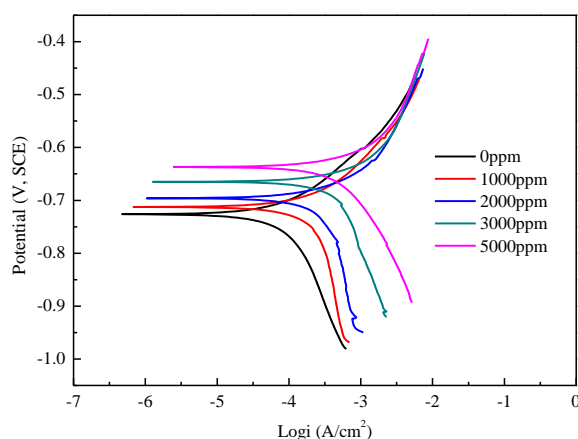


Figure 7. Polarization curves of 3Cr steel at 50°C in the CO₂-saturated oilfield formation water with different acetic acid concentrations

Table 3. Electrochemical parameters at different acetic acid concentrations based on polarization curves

Acetic acid concentration (ppm)	$E_i = 0$ (mV, SCE)	b_a (mV/dec)	b_c (mV/dec)	i_{corr} ($\mu\text{A}/\text{cm}^2$)
0	-0.726	115	359	95.68
1000	-0.712	134	699	238.25
2000	-0.696	154	657	429.26
3000	-0.665	184	308	619.91
5000	-0.637	180	271	801.10

Figure 8 presents the Nyquist diagrams of 3Cr steel at 50°C in the CO₂-saturated oilfield formation water with different acetic acid concentrations. Large and small diameters of the capacitive loop at high and low frequencies, respectively, are visible for the specimen at 0 ppm of acetic acid concentration. The high-frequency capacitive loop is mainly considered the capacitance of the double

electrode layer between the corrosion scale and the solution. The low-frequency capacitive loop is primarily associated with the adsorption characteristics of the intermediate corrosion scale [24]. As the acetic acid concentration increased, the diameter of the high-frequency capacitive loop decreased; moreover, as the low-frequency capacitive loop gradually disappeared, the inductive loop rose in the high acetic acid concentration. Zhu [11] also reported similar results when studying the effect of acetic acid concentration on the corrosion of N80 carbon steel in oil field formation water containing CO₂.

Figure 9 presents an equivalent electrical circuit fitting the EIS data of 3Cr steel at 50°C in the CO₂-saturated oilfield formation water with different acetic acid concentrations. This result is in agreement with that of Zhu [11] who reported that R_s is the solution resistance, C_{dl} is the double-layer capacitance between corrosion scales and solution, R_t is the charge-transfer resistance, R_L is the inductive resistance, L is the inductance related to the dissolution of corrosion scales, Q_c is the constant phase element representing double-layer capacitance, and R_c is the corrosion scale resistance. The fitted Nyquist diagrams are presented in Fig. 10, exhibiting high fitting accuracy. The fitting results are provided in Table 4. As can be seen from Table 4, the charge-transfer resistance R_t decreased in tandem with an increase in acetic acid concentration. Moreover, the corrosion scale resistance R_c after adding acetic acid decreased compared with the value without adding acetic acid.

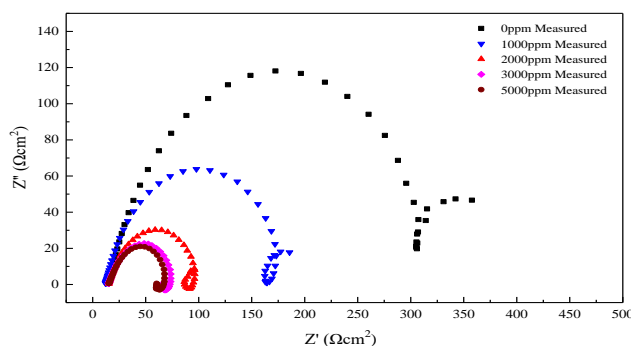


Figure 8. Nyquist diagrams of 3Cr steel at 50°C in the CO₂-saturated oilfield formation water with different acetic acid concentrations

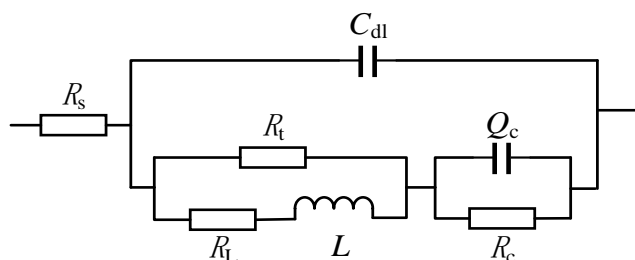


Figure 9. Equivalent electrical circuit for 3Cr steel at 50°C in the CO₂-saturated oilfield formation water

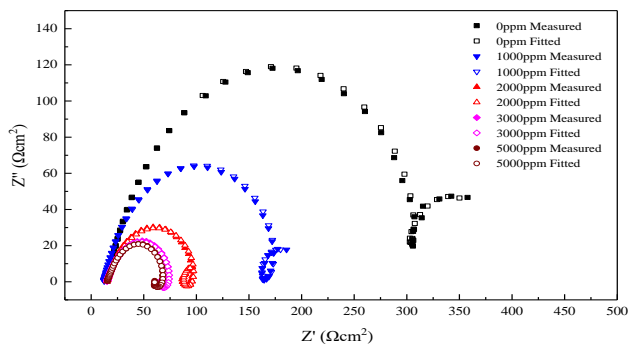


Figure 10. Fitted Nyquist diagrams of 3Cr steel at 50°C in the CO₂-saturated oilfield formation water with different acetic acid concentrations

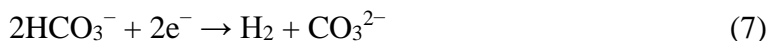
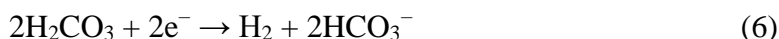
Table 4. Values of equivalent electrical circuits for 3Cr steel at 50°C in the CO₂-saturated oilfield formation water with different acetic acid concentrations

ppm	$R_s(\Omega \text{ cm}^2)$	$C_{dl}(\text{F cm}^2)$	$R_t(\Omega \text{ cm}^2)$	$R_L(\Omega \text{ cm}^2)$	$L(\text{H cm}^2)$	$Q_c(\text{F cm}^2)$	$R_c(\Omega \text{ cm}^2)$
0	15.49	5.90 E-4	327.7	2.15 E3	3.11 E3	0.144	88.66
1000	12.17	7.85 E-4	183.7	773.2	853.9	0.384	35.6
2000	15.06	1.29 E-3	93.97	314.1	344.7	1.10	15.89
3000	14.98	7.48 E-4	13.52	7.06 E-3	9.25	3.54 E-4	51.19
5000	15.23	8.21 E-4	13.34	3.19 E-5	8.53	5.53 E-4	49.21

4. DISCUSSION

4.1. Corrosion mechanism of 3Cr steel in the CO₂-saturated oilfield formation water without acetic acid

As for CO₂ corrosion without acetic acid in the oilfield formation water, many researchers have examined the electrochemical reactions. The CO₂ corrosion reaction mechanism on the 3Cr steel surface in the CO₂-saturated solution is as follows [25]:



Specimen profilometry images (Fig. 4a) and PR (Fig. 7) show equal corrosion depth, with the PR value being close to 1, which means that uniform corrosion occurred on the surface of the specimen in the CO₂-saturated solution without acetic acid.

As for corrosion products, the analyses of the elemental composition and XRD patterns of the corrosion scales of 3Cr steel in Table 2 and Fig. 3 reveal that the dominating phase may be FeCO₃ of corrosion scales by reaction (8) [23]. The image of microscopic morphologies (Fig. 2a) characterizes the closely and evenly distributed FeCO₃ corrosion scales.



In addition, Guo's results indicate that the corrosion products of Cr steel contain $\text{Cr}(\text{OH})_3$ alongside FeCO_3 [22]. The results of the EDS show the partial existence of the Cr element amounts. That Cr element is more active than the Fe element poses a huge threat to the life of 3Cr steel, leading to the dissolution of Cr element in the solution. However, the addition of Cr element extends the service life of carbon steel for the formation of $\text{Cr}(\text{OH})_3$ on the surface of the steel in the CO_2 -saturated solution by reaction (9). Similar to Muraki [26], Xu [12] perceived this result as having excellent stability and compactness, covering the whole steel surface and reducing the corrosion rate.



4.2 Corrosion mechanism of 3Cr steel in the CO_2 -saturated oilfield formation water with acetic acid

With the absence of acetic acid in the CO_2 -saturated oilfield formation water, the main reactions (5)–(7) dominate the cathodic reaction process, and the main product of the cathode contains HCO_3^- and CO_3^{2-} . However, the presence of acetic acid induces a more complex electrochemistry reaction and a new reduction reaction of the cathode, as presented below:



In this work, the weight loss tests (Fig. 1) revealed that the presence of acetic acid greatly affected and stimulated the general corrosion rate. The results of the polarization curves also revealed that the addition of acetic acid promotes the corrosion reaction, especially in the cathodic reaction process. Hedges pointed out that the reduction reaction (10) of acetic acid is the main process in the solution [27]. All these results strongly suggest that the addition of acetic acid reduced reaction (10) and promoted the cathodic reaction process.

The impedance spectrum data (Fig. 9) revealed that the high-frequency capacitive loop diameter decreased, and the low-frequency capacitive loop gradually disappeared, which is consistent with the polarization curve results and the weight loss tests. The fitted data in Table 5 show that the charge-transfer resistance R_t and the corrosion scale resistance R_c after the addition of acetic acid decreased compared with the values obtained without the addition of acetic acid. These findings suggest that acetic acid accelerates the corrosion reaction process by influencing the charge-transfer of cathode by reaction (10) [23]. Moreover, the disappearance of the low-frequency capacitive loop and the change in the corrosion scale resistance R_c indicate that acetic acid affects the adsorption process of the corrosion product scales. Other researchers obtained similar results [2] [15]. They revealed that the dissolution and adsorption process of the corrosion product film shown in reactions (11)–(13) occurred in the solution. Evidently, the greater the acetic acid concentration, the harder the formation of the corrosion product film.



In conclusion, two main factors had an impact on acetic acid after being added to the solution. The first factor is that the reduced reaction of acetic acid participates in the cathodic reaction, which

stimulates the corrosion reaction. The other factor is that acetic acid influences the adsorption process of the corrosion product scales. This results in the exposure of the steel substrate to the solution without the protection of the corrosion scales, thus increasing the general corrosion rate. Moreover, these two factors are more severe when the acetic acid concentration increases.

4.3 Acetic acid effect on localized corrosion

According to the specimen profilometry images (Fig. 4), the calculation of the localized corrosion rate (Fig. 5), and the PR value (Fig. 6), in the absence of acetic acid, the corrosion form is uniform, and no localized corrosion occurs on the surface of the 3Cr steel substrate. However, as the acetic acid concentration increased, the specimen profilometry images (Fig. 4) showed that small pits gradually appeared on the surface of the steel and gradually expanded outward into larger pits; moreover, the Cr elements on the surface of the steel also exhibited a serious uneven distribution. In addition, the localized corrosion rate (Fig. 6) gradually increased, with the PR value (Fig. 7) being far from 1. These results indicate that acetic acid causes the localized corrosion to occur on the surface of 3Cr steel, suggesting that the higher the acetic acid concentration, the more serious the localized corrosion.

Curious about the influence of acetic acid on the localized corrosion of 3Cr steel, the authors developed a pitting development model to explain the localized corrosion mechanism. Some small, uneven areas exist on the surface of the sample steel due to the roughness of steel processing. The ingress of acetic acid causes the uneven pit areas of the steel surface to be filled with acetic acid and formation water. As presented in Fig. 11(a), corrosion reaction occurs on the steel surface. As presented in Fig. 11(b), Amri [28] pointed out that acetic acid concentration decreases as the depth of the pit increases (see Fig 11(b)). Arguably, there is a difference in the acetic acid concentration gradient and corrosion potential gradient between the pithead and the bottom of the pit, which causes a corrosion micro battery to occur on an uneven area. While the anode reaction occurred at the bottom of the pit, the cathodic reaction occurred on the pithead. As presented in Fig. 11(c), the vertical depth of the uneven pit area increasingly deepened until the acetic acid at the bottom of the pit was consumed. More importantly, when the solution contains Cl^- , it can induce, activate, and stimulate localized corrosion on the surface of the sample. Cl^- in the solution is not the dominant factor for corrosion because the smaller and more active chloride ions can be selectively adsorbed on a layer of corrosion product film on the surface of the sample [29]. The oxygen atom is combined with the cations in the corrosion product film to form soluble chloride. The reaction of chloride hydrolysis is (14)–(16). The H^+ generated during the hydrolysis reduces the pH of the solution, which means that the solution in the pit is acidified. As the pore corrosion progresses, the H^+ concentration in the pore increases, whereas the pH value decreases continuously. In this highly aggressive medium condition, the metal in the pores remains active and dissolved, and the pore corrosion continues to develop, thus forming localized corrosion on the substrate. The hydrolyzed Cl^- can return to the sample surface in the electric field; it also continues to activate the sample surface and further develops corrosion. The combined effect of these two aspects stimulates the formation and development of localized surface corrosion. As presented in Fig. 11(d), the pit will eventually be

corroded into a larger one. This result will take a more serious shape with an increase in the solution’s acetic acid concentration.

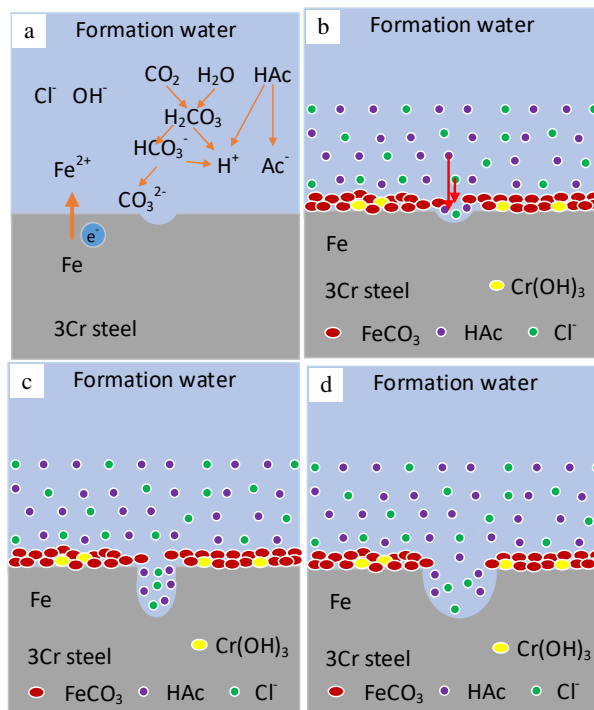
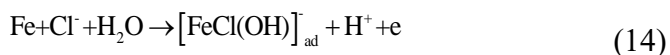


Figure 11. Schematic diagram of localized corrosion development model with acetic acid

5. CONCLUSION

The effect of acetic acid on the localized corrosion mechanism of 3Cr steel at 50°C in the CO₂-saturated oilfield formation water was investigated, and the following conclusions were drawn:

(1) In the absence of acetic acid, the produced corrosion scales of the iron carbonate layer covering the surface of the 3Cr steel specimen were amorphous and continuously close. As the acetic acid concentration increased, the corrosion scales gradually became looser and shed off.

(2) In the presence of acetic acid, the general corrosion rate and the localized corrosion rate increased considerably as acetic acid concentration increased. The reduced reaction of undissociated acetic acid in the solution participated in the process of the cathodic corrosion reaction, and the acetic acid affected the adsorption process of the corrosion product scales, accelerating the entire corrosion reaction.

(3) Acetic acid significantly contributed to the generation of localized corrosion on the surface of 3Cr steel. A corrosion micro battery occurred due to the difference in acetic acid concentration in the

small pit on the surface of the steel under the common effect of Cl^- , which caused severe localized corrosion on the surface of 3Cr steel.

ACKNOWLEDGMENTS

This work was funded by the National Natural Science Foundation of China, its grant number is 51674212.

References

1. D. A. López, S. N. Simison and S. R. de Sánchez, *Electrochim. Acta.* 48(2003)845.
2. G. A. Zhang and Y. F. Cheng, *Corros. Sci.*, 51(2009)87.
3. M. B. Kermani, M. Dougan, J. C. Gonzales, C. Linne and R. Cochrane, *NACE International*, Houston, Texas(The United States), 2001.
4. D. A. López, T. Pérez and S. Simison, *Mater. Des.*, 24(2003)561.
5. Y. Xie, L. Xu, C. L. Gao, W. Chang and M. X. Lu, *Mater. Des.*, 36(2011)54.
6. S. Q. Guo, L. N. Xu, L. Zhang, W. Chang and M. X. Lu, *Corros. Sci.*, 63(2012)246.
7. L. N. Xu, S. Q. Guo, W. Chang, T. H. Chen, L. H. Hu and M. X. Lu, *Appl. Surf. Sci.*, 270(2013)395.
8. Q. L. Wu, Z. H. Zhang, X. M. Dong and J. Q. Yang, *Corros. Sci.*, 75(2013)400.
9. R. Elgaddafi, A. Naidu, R. Ahmed, S. Shah, S. Hassani, S. Osisanya and A. Saasen, *J. Nat. Gas Sci. Eng.*, 27(2015)1620.
10. Z. F. Yin, X. Z. Wang, L. Liu, J. Q. Wu and Y. Q. Zhang, *J. Mater. Eng. Perform.*, 20(2011)1330.
11. S. D. Zhu, A. Q. Fu, J. Miao, Z. F. Yin, G. S. Zhou and J. F. Wei, *Corros. Sci.*, 53(2011)3156.
12. L. N. Xu, B. Wang, J. Y. Zhu, W. Li and Z. Y. Zheng, *Appl. Surf. Sci.*, 379(2016)39.
13. L. Dominique and G. M. Yves, *NACE International*, Orlando, Florida(The United States), 2000.
14. J. Crolet, A. Dugstad and N. Thevenot, *Corrosion*, San Antonio, Texas(The United States), 1999.
15. G. A. Zhang and Y. F. Cheng, *Corros. Sci.*, 51(2009)1589.
16. A. N. Omkar and S. Nescic, *NACE International*, Houston, Texas(The United States), 2005.
17. P. C. Okafor and S. Nescic, *Chem. Eng. Commun.*, 194(2007)141.
18. M. H. Nazari and S. R. Allahkaram, *Mater. Des.*, 31(2008)4290.
19. ASTM, G1. "Standard practice for preparing, cleaning, and evaluating corrosion test specimens." American Society for Testing and Materials, 2003.
20. N. R. Rosli, S. Nescic, Y. S. Choi and D. Young, *NACE International*, Vancouver, British Columbia(Canada), 2016.
21. Z. J. Jia, X. G. Li, C. W. Du, Z. Y. Liu and J. Gao, *Mater. Chem. Phys.*, 132(2012)258.
22. T. H. Chen, L. X. Xu, M. X. Lu, W. Chang and L. Zhang, *NACE International*, Houston, Texas(The United States), 2011.
23. M. H. Nazari, S. R. Allahkaram and M. B. Kermani, *Mater. Des.*, 31(2010)3559.
24. M. Keddad, O. R. Mattos and H. Takenouti, *J. Electrochem. Soc.*, 128(1981)257.
25. M. Ueda and A. Ikeda, *NACE International*, Denver, Colorado(The United States), 1996.
26. T. Muraki, T. Hara and H. Asahi, *NACE International*, Denver, Colorado(The United States), 2002.
27. B. Hedges and L. McVeigh, *NACE International*, San Antonio, Texas(The United States), 1999.
28. J. Amri, E. Gulbrandsen and R. P. Nogueira, *Electrochem. Commun.*, 10(2008)200.
29. N. Y. Zhang, D. Z. Zeng, G. Q. Xiao, J. F. Shang, Y. Z. Liu, D. C. Long, Q. Y. He and A. Singh, *J. Nat. Gas Sci. Eng.*, 30(2016)444.